METHODOLOGY OF ARM DESIGN FOR MOBILE ROBOT MANIPULATOR USING TOPOLOGICAL OPTIMIZATION

ZBYNEK PASKA[1]**, JAROSLAV ROJICEK**[1]**, PETR FERFECKI**[1]**,
MARTIN FUSEK**[1]**, DOMINIK HECZKO**[2]**, VACLAV KRYS**[2]

[1]Department of Applied Mechanics, Faculty of Mechanical Engineering, Ostrava-Poruba, Czech Republic

[2]Department of Robotics, Faculty of Mechanical Engineering, Ostrava-Poruba, Czech Republic

The contribution deals with the problematics of topology optimization of the arm of a mobile robot manipulator for the international competition European Rover Challenge (ERC). The manipulator was designed at the Department of Robotics at VSB - TU Ostrava and is described in detail below. The aim was to test the entire design process: determination of loading forces, material model and parameters identification, maximal allowed stress in the structure, the topology optimization and the manufacturing process of the arm by FDM additive technology. The process has been tested for his future automation. The aim was also to create the new arm lighter than the original one, but the reliability must be satisfied.

KEYWORDS

topology optimization, manipulator arm optimization, material model, DIC, ABS-M30, 3D print, FDM additive technology

1 INTRODUCTION

This article was created within the project 'Research Centre of Advanced Mechatronic Systems', which is solved at VSB-TU Ostrava. One task of the project is to optimize robot arms according to a manipulation cycle conditions. The new optimal arm design must satisfy the operating conditions, it must withstand the loads and mostly there is the requirement to made it with minimal weight.

The main task is to test the procedure that would lead to automatic manipulator design. This type of a methodology can be divided into five basic steps:

1) Assignment of keys information for an automatic design (loadings, material information, flanges or connection types etc.). This step is preliminary phase of the methodology.
2) Design of the arm optimization area,
3) Optimal arm design – topology optimization,
4) Adjustment of topological design for validation calculation and 3D printing,
5) Production technology – 3D printing.

A mobile robot for the international competition European Rover Challenge (ERC) [ERC 2020] is a test example for testing functionality of proposed design and manufacturing process. This testing example shows some problems related with pre-made flanges, available material models and their parameters with regards to the wide range of materials (especially for additive technology). The testing task for topology optimization is to design the arm of the manipulator from plastic material ABS-M30 and manufactured by FDM additive technology [Dizon 2018]. The original arm consisted of tube and 2 flanges and was made of aluminium alloy Al6061.

The first step was to determine the loading forces acting on the arm. The measurement was carried out under laboratory conditions and was intended to replace the real operation conditions. In the case of manipulators, it is also necessary to consider the dynamic behaviour of the individual drives, joints - bearings, stiffness of the manipulator arms etc. [Tafazoli 1999], [Corradini 2012], [Zhang 2007].

Equally important step is determination of printed materials and investigation of its properties (material model, material parameters and permissible stress values). For some 3D printed materials, they can show relaxation/creep/ratcheting [Zhang 2018] even at room temperature, the behaviour of the resulting components may not be isotropic [Duty 2018]. A different loading cases were carried out on the specimens in order to determine the material parameters. There was used Digital Image Correlation method (DIC) [Schreier 2009] to determine the Poisson ratio.

Topology optimization is an additional process in the design of mobile robot manipulator. Topology optimization would be the part of the whole design process, which will consider purpose of the robot, its workspace, loadings, trajectories and other conditions, e.g. dynamic parameters. Several methods of topological algorithms can be found in the literature (density approach, level set method, evolutionary approaches etc.) [Sigmund 2013], [Bensoe 2003]. Topology optimization of the arm was performed in Ansys 2019 R3 software. The goal of topological optimization is to find a structure that appears to be the most efficient based on predefined criteria. In topological optimization, the target function is minimized, but the constraint conditions must be satisfied [Ansys 2019].

Chapter 2 described basic information about the mobile robot with the manipulator. In the next two chapters are shortly described topology optimization method and basics about DIC method. In chapter 5 is presented determining of loadings by measurement of accelerations on the mobile robot and its arm. Material model identification (with its parameters) from the set of tension experiments is described in chapter 6. Chapter 7 describes the input for the optimization, defines the boundary shape of the arm and shows the optimization settings. In addition, different shapes of the topological optimization arm are shown schematically. The two resulting shapes are shown in more detail. There is also a photo of the arm, which was made with additive technology. In conclusion, the whole process is described, a critical point is identified, and further actions are proposed.

2 MANIPULATOR ERC

The manipulator was designed for a mobile robot competition European Rover Challenge (ERC) [ERC 2020]. It is a rover competition on Mars–simulated environment. Rover must complete all of tasks: science task, maintenance task, collection task and traverse task. Each task has several goals. Rover is controlled in real time from operator centre. The operator does not have direct view on the rover, there are allowed feedback from sensory subsystem (cameras, proximity sensors etc.) only.

2.1 Science task

The aim of this task is to obtain three samples of 'Martian soil'. Each sample is taken from a different location and different geological layers. Manipulation with samples is illustrated in Fig. 1.

Figure 1. Sample collecting.

2.2 Maintenance task

In this task the remote operation with a control panel (shown in Fig. 2) on which several switches, levers, buttons and other electrical components are mounted on is simulated. These components must be set to the desired state by arm manipulation.

Figure 2. Arm manipulation on the control panel (maintenance task).
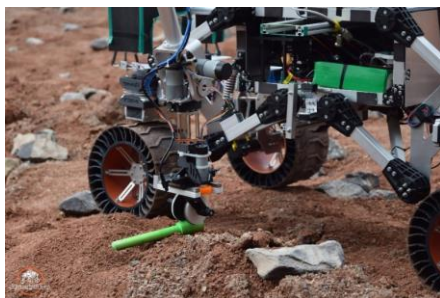
Figure 3. Manipulation with cache (collection task).

2.3 Collection task

The aim of this task is to find, pick up, store in on-board containers and transport the aluminium caches (as seen in Fig. 3) with rule-defined dimensions. Caches are represented as green cylinder of maximal 30 mm diameter and 200 mm length. Weight of cache should be fewer than 300 g and centre of gravity is unknown. The vertical reach of the arm from the ground is 1.5 m. The manipulator must be able to store three samples. A rock sample weighing 100 g, an above-ground soil sample weighing 200 g and an underground soil sample weighing 25 g.

2.4 Mechanical part

Design specifications of the manipulator are based on goals of each task specified by rules of this competition. Design of the

manipulator was made from the last joint (J5) to the base, because of known loads. At the end of the manipulator there are gravitational and inertial forces from the end–effector and manipulated object. The last joint must rotate the end–effector in order to set the three-phase switch to ON position (measured 1.5 N m). Kinematics solution and axial distances of the manipulator are shown in Fig. 4. There was used angular kinematics, inspired by [Mohammed 2010].
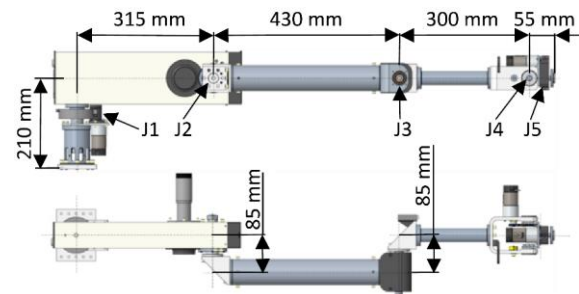

Figure 4. Basic manipulator dimensions. The focus is on the arm between joints J3 and J4.

In order to lightweight manipulator design, links between joints were made of normalized aluminium profiles (EN-AW6060) and supported parts were made of aluminium blocks (EN-AW6063). Gears which are the most stressed via torque transmission are made of steel. Gears in joint J5 and J4 are made of steel ETG 100, other gears are made of steel C43. Plastic covers and sensor holders are 3D printed parts (polycarbonate). The manipulator is manually controlled in real time. It does not execute the same motion sequence as an industrial robot, so that high positioning accuracy is not required. Technical parameters of the manipulator are specified in the Tab. 1.

Weight of the manipulator	10.5 kg
Load capacity	1 kg
Maximum reach	890 mm
Max. acceleration	0.5 m s^{-2}
Max. speed of TCP (Tool Center Point)	1 m s^{-1}

Table 1. Technical parameters of the manipulator.

3 TOPOLOGICAL OPTIMIZATION

In this contribution, topological optimization was used to find the most suitable geometrical shape of the parts regarding to its loading, mass distribution and boundary conditions. The method 'Solid Isotropic Material with Penalty' (SIMP) based on principle 'density approach' will be described below in the article [Andreassen 2011]. SIMP method is available in Ansys 2019 R3 software [Ansys 2019].

To each FEM element is assigned a design variable called material relative density factor x_e. The density of the elements can range from 0 to 1 (continuously changing value). It is not the physical density of the material, but variable that determines the importance of the element in the structure. The Young's modulus for each element is determined as:

$$E_e = x_e^p \cdot E_0, \tag{1}$$

where E_e is Young's modulus of the element; E_0 is Young's modulus of the original material; p is penalty factor and x_e is material relative density factor.

There are many problems with topological optimization. For example, there may occurred problem called 'checkerboard problem'. It is the layout of the structure into a chessboard shape in certain parts of the part. Another problem is to establish a connection between two elements if they are not connected in an enough number of nodes.

One possible solution is to use filters. These solutions are not mathematically confirmed, but a several numerical experiments confirm that the result can be considered as an optimal shape. Another modification is the addition of the Young's modulus of the 'turned-off' element. This modification will reduce the risk of developing a singular stiffness matrix. Young's modulus for each element is than in the form:

$$E_e = E_{min} + \tilde{x}_e^p \cdot (E_0 - E_{min}), \qquad (2)$$

where $\tilde{x}_e$ is a filtered material relative density factor; E_{min} is Young's modulus of 'turned-off' element.

For example, if the numerical scheme results in a black and white design, the designer may choose to ignore the physical importance of the transitions that are grey. The question of physical relevance is often mentioned because many interpolation computational procedures do not get rid of completely grey. Also, the physical execution of possible designs plays a role in interpreting results from a prematurely terminated optimization algorithm that did not fully converge in the range 0 to 1. In order to treat the SIMP as a material model, penalty factor must meet the following requirements:

$$p \geq \max\left\{\frac{2}{1-\mu}, \frac{4}{1+\mu}\right\}, \text{ (in 2D)}, \qquad (3)$$

$$p \geq \max\left\{15\frac{1-\mu}{7-5\mu}, \frac{3}{2}\frac{1-\mu}{1-2\mu}\right\}, \text{ (in 3D)}, \qquad (4)$$

where μ is Poisson ratio. For example, steel has Poisson ratio $\mu = 0.3$, so the penalty factor can be equal to 3.

4 DIGITAL IMAGE CORRELATION (DIC)

DIC measurements are non-destructive methods that do not affect the measured component. It allows to determine measured quantities on the whole captured specimen surface. It is basically divided into 2D DIC method (using one camera) and 3D DIC method (here it is necessary to use at least 2 cameras (stereoscopic system) [Schreier 2009]. Mercury RT® system (2x2.3Mpx@40Hz) provided by Sobriety s.r.o. company was used for measurement (see Fig. 5.) [Sobriety 2012].

Figure 5. Mercury RT® system.

The principle of the method is based on correlation algorithm. This method compares images of the surface of a specimen during the loadings. Speckle pattern must be created on the captured specimen surface. The comparison of images takes place in smaller areas called facets. The random pattern makes each facet unique. There are several correlation algorithms based on finding extremes of correlation functions corresponding facets [Trebuna 2017].

5 LOADING STATES DETERMINATION

The arm load can be divided into two types. The first is a static load. The static load is calculated from the weight of the effector and the weight of things the effector holds (assuming a maximum manoeuvrable weight of 1 kg) and the torque that the manipulator must exert to turn off the rotary electrical switch. The second type of load arises from dynamic effects (when starting, braking and changing the direction of movement of some part of the manipulator). The maximum possible horizontal and vertical movement speed is assumed. Dynamic overload was measured using an accelerometer.

The centre of gravity is determined from the CAD model and includes the mass of the effector (which consists of many components of different material) and the mass of the manipulated things attached to the effector. The position of the centre of gravity is shown in Fig. 6.
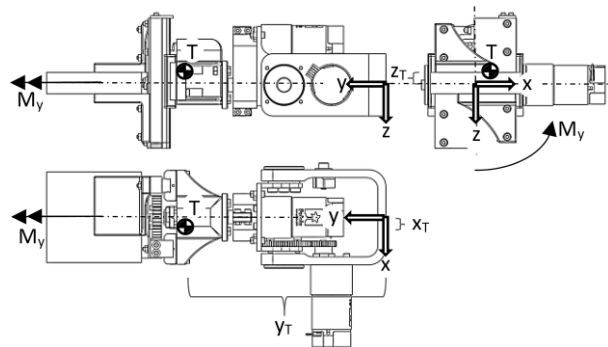

Figure 6. Position of the centre of gravity: $x_T = 6.7$ mm; $y_T = 161.8$ mm; $z_T = -5.2$ mm. The torque value is $M_y = 1.5$ N m.

The total weight of the effector including the manipulated load is $m_c = 2.821$ kg.

The dynamic arm load was determined by measuring possible modes of manipulator and arm behaviour. Measurements were performed with a three-axis accelerometer and measuring device Brüel & Kjær (B&K - Type 3560C, universal high-speed analyser, 4/2 channel module: B&K - Type 3109, LAN interface module: B&K - Type 7533, S/N 2348762). An accelerometer 'Triaxial DeltaTron' type 4524B was used (Fig. 7, 8).

Acceleration timestamp was recorded for a total of 7 operating mode. Tab. 2 shows the short description of the modes and the maximum acceleration values measured for each load mode. We only provide a graphical record for one example, which are briefly described below. The movement in all cases was performed with the maximum possible acceleration of the engines and a sudden stop at the end of the movement. Real manipulation task takes 1-5 minutes and includes modes 1-6, mode 7 - the ride only takes place when the arm is folded. Modes 2-7 were included to the evaluation, because even in the manipulation task only a small amount of travel can be made.
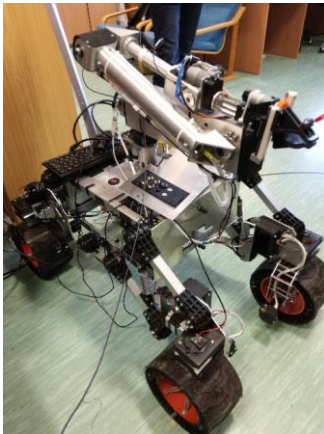
Figure 7. Measuring equipment.

Figure 8. Manipulator in starting position.

Mode 1) extending arm to working position	$a_{c1,max} = 0.59$ m s^{-2}
Mode 2) movement vertically by 90° - joint J3	$a_{c2,max} = 0.51$ m s^{-2}
Mode 3) movement vertically by 90° - joint J2	$a_{c3,max} = 0.62$ m s^{-2}
Mode 4) movement horizontally by 90° - joint J1	$a_{c4,max} = 0.53$ m s^{-2}
Mode 5) movement vertically by 90° - joint J4	$a_{c5,max} = 0.80$ m s^{-2}
Mode 6) rotation about horizontal axis by 90°- joint J4	$a_{c6,max} = 0.36$ m s^{-2}
Mode 7) driving on smooth surfaces	$a_{c7,max} = 0.61$ m s^{-2}

Table 2. Maximum acceleration values.

In Fig. 9, 10, 11, 12 are depicted the components of the acceleration and total absolute value of the acceleration for first testing mode.
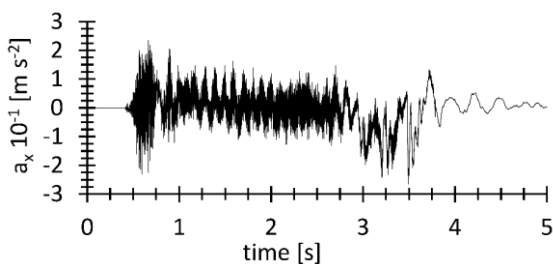
Figure 9. Accel. component a_x, of mode 1.
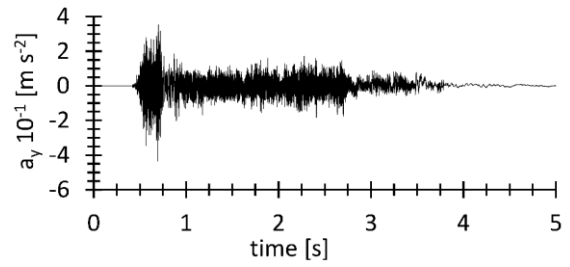
Figure 10. Accel. component a_y, of mode 1.
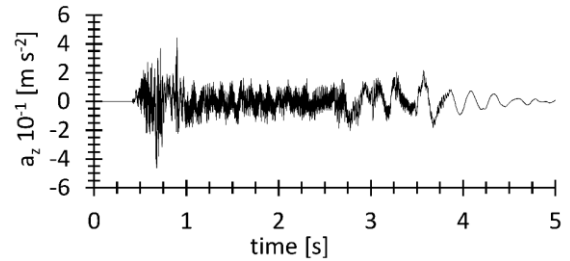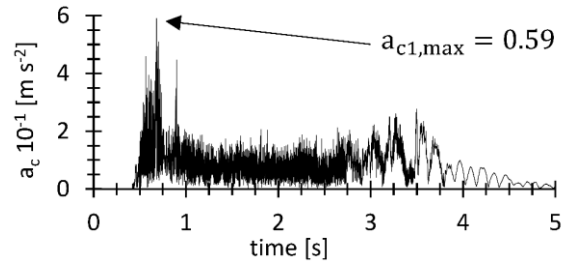

Figure 11. Accel. component a_z, of mode 1.

Figure 12. Accel. component a_C, of mode 1.

Let the total force be given by:

$$\mathbf{F} = m_c\,\mathbf{a}\,, \tag{5}$$

where $m_c = 2.821$ kg is the total mass of the effector including the weight of the load, $\mathbf{a}$ is the total maximum acceleration or deceleration. The total maximum acceleration is simply determined as the sum of the individual total maximum accelerations (see Tab. 2) from measurements 2 to 7 according to equation (6):

$$a_{c,max} = \sum_{i=2}^{7} a_{ci,max} = 3.5 \cong 4\ \text{m s}^{-2}. \tag{6}$$

The procedure for calculating the maximum acceleration value is very simplified. The actual acceleration value shall always be less than or equal to the maximum calculated value.

The resulting load force F is given by the superposition of static and dynamic load, acting at the centre of gravity and is given by:

$$F = G + D = m_c\,g + m_c\,a_{c,max} = 38.96 \cong 39\ \text{N}, \tag{7}$$

where g is the value of the acceleration of gravity.

The measurement also showed that critical values occur at the beginning of the movement (see Fig. 9, 10). The maximum value of acceleration was found during the initial movement of the arm in most of the tested modes. The measurement was performed at maximum movement speeds and the movement time did not exceed 10 s. Standard arm handling tasks can take 1-5 minutes. The operator of the tested modes was a human, in some cases it may be replaced by another operator or, for example, a neural network that is currently unavailable.

The proposed procedure is very simple, and it can give incorrect acceleration values. The procedure will need to be further developed and refined.

6   NEW MATERIAL OF THE ARM

The original arm is made of aluminium alloy and is to be replaced with ABS-M30 plastic. The manufacturer does not mention the Poisson ratio. According to the manufacturer, the Young's modulus is in the range $E = 2180$ MPa to $E = 2230$ MPa. For the material tests the shape of the specimens according to Fig. 13 was used. The shape of the specimen was designed with regards to the use of the DIC measurement method so that damage occurs in the middle of the specimen.
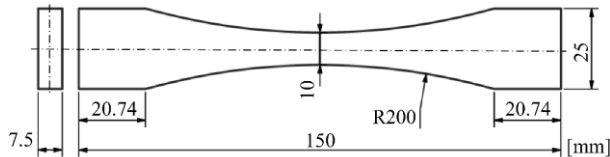
Figure 13. Specimen scheme.

The time dependence of the material behaviour and the method of laying of material layers were tested on the same specimen shapes. The method of laying layers of material in 3D printing for three specimens is shown in Fig. 14. Each specimen was progressively elongated with a 0.25 mm displacement step and then held in this position for 60 s to at least partially capture the stress relaxation (see Fig. 15).
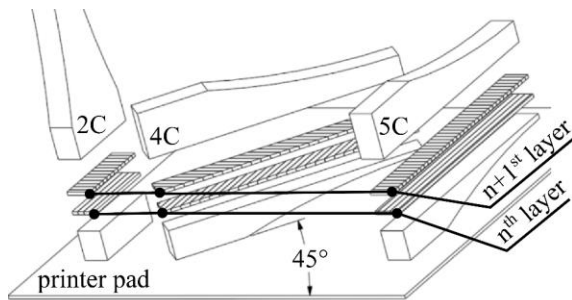

Figure 14. Method of laying of material during 3D printing.
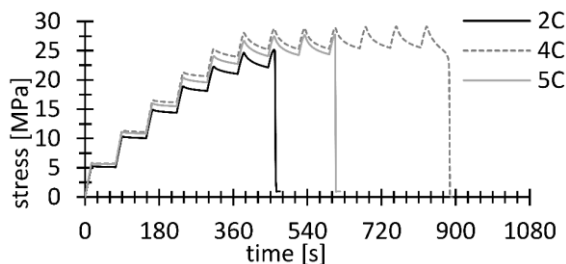

Figure 15. Progressive tensile test record for three specimens.

As can be seen up to a certain stress value, the time delay does not have significant influence on it. Up to approximately 10 MPa, there is no significant stress relaxation even though the time of 60 s is relatively short. Stress value 10 MPa was chosen as the limit value for further analyses. There should be no significant signs of relaxation within 1 to 5 minutes.
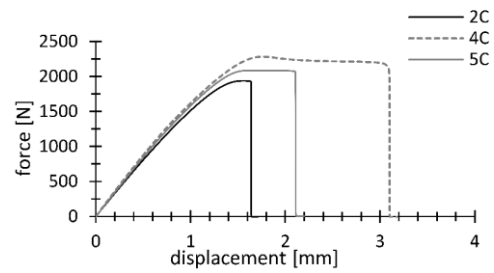

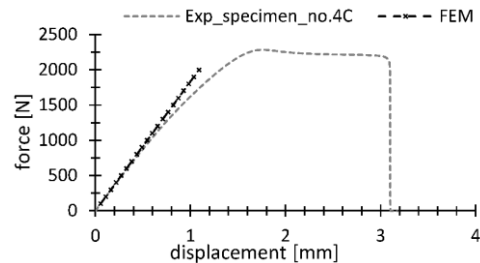**Figure 16.** Tensile test for three specimens.

Figure 17. Young's modulus determination.

From Fig. 15, 16, 17 can be seen that up to about 10 MPa (750 N) the material behaves linearly elastically. The value of Young's modulus is almost identical in the monitored area for different orientation of material laying during printing. The material is therefore considered isotropic and homogeneous. More detailed analysis of material behaviour at higher loads (relaxation, creep, orthotropic behaviour, etc.) will be discussed in a future article. From DIC measurements it is relatively easy to determine the Poisson ratio. The value of the Poisson ratio is $\mu = 0.33$. The value of Young's modulus is $E = 1950$ MPa.

7   TOPOLOGY OPTIMIZATION OF THE MANIPULATOR'S ARM

In order to perform topological optimization, we decided to use the possibilities of Ansys software. The SIMP method used is briefly described in the chapter 3. An envelope (optimization space) was designed to meet all the technical requirements for the arm (cable space, collision between manipulator members, etc.). The designed envelope is limited by flange shapes that define the built-in space, including the cable space. The original shape of the arm is shown in Fig. 18, a modified model for topological optimization is shown in Fig. 19.

The new arm will be made of ABS-M30, whose behaviour (material model including parameters) was analysed in the chapter 6. This plastic is modelled using a homogeneous, linearly elastic and isotropic material model.

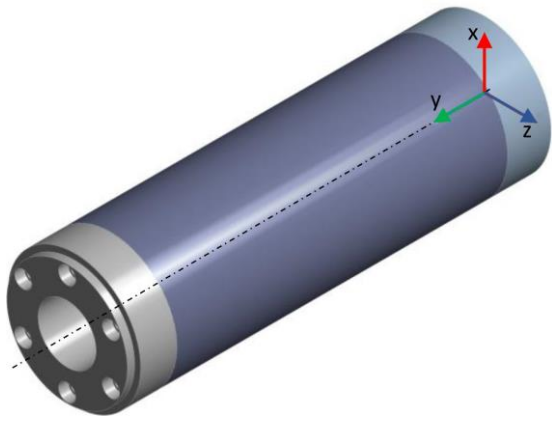**Figure 18.** Original shape of the manipulator arm.

Figure 19. Modified model of the arm for optimization.

Boundary conditions and load forces are applied to the flanges (see Fig. 20). On the right side is flange fixed on the whole surface, on the left side is on the flange surface applied torque 1.5 Nm and force 39 N in centre of gravity of effector.
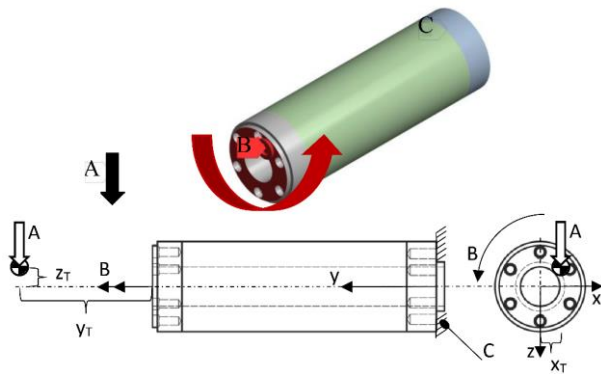

Figure 20. A – load force 39 N; B – torque 1.5 N m; C – fixed support condition.

The FEM model contains 162 633 nodes, 40 195 elements (37 150 Solid186 + 3 045 Solid187), see Fig. 21. The optimization space is displayed brighter.
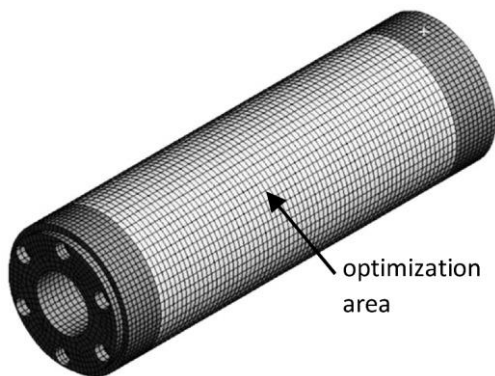

Figure 21. FEM model for optimization.

The previous chapters show two key criteria for topological optimization:
1) The weight of the plastic arm must be less than the weight of the original aluminium alloy arm (minimizing the weight of the arm),
2) The mechanical stress must not exceed 10 MPa (maximum value of the reduced equivalent stress).

The solution was done in setting the target function to maximize the stiffness matrix of the component while reducing the weight of the arm. The following variants were compared:
a) original shape with aluminium alloy material,
b) original shape with plastic material,
c) envelope shape with plastic material,
d) 3 x optimized shape with plastic material - the first has the weight 0.214 kg and the others have a lower weight (0.178 kg and 0.139 kg).

Individual shape designs are shown in Tab. 3. The table shows the weight for each variant, first natural frequency, maximal absolute displacement and maximal HMH stress.

The proposed iterative optimization approach determined by the percentage of the weight of the arm can be easily algorithmized and it seems to be the most suitable regarding expected optimization conditions. The optimized model is further modified (smoothing the shape, removing various shape defects, etc.) for control FEM calculations. Shape modifications of the model in .stl format can be done directly in Ansys in SpaceClaim module.
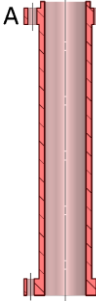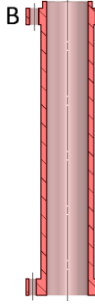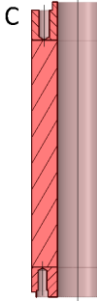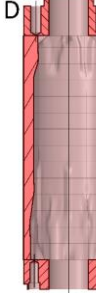
	A	B	C
Material	Al6061	ABS-M30	ABS-M30
Weight	0.211 kg	0.084 kg	0.360 kg
1st natural frequency	3745 Hz	983 Hz	1882 Hz
Max. displacement	0.072 mm	2.641 mm	0.176 mm
Max. HMH stress	14.0 MPa	16.8 MPa	1.3 MPa
	D	E	F
Material	ABS-M30	ABS-M30	ABS-M30
Weight	0.214 kg	0.178 kg	0.139 kg
1st natural frequency	1733 Hz	1378 Hz	745 Hz
Max. displacement	0.277 mm	0.342 mm	0.649 mm
Max. HMH stress	1.7 MPa	2.0 MPa	11.0 MPa

Table 3. Proposed design shapes.

The key values for selecting the resulting variant are the weight and the maximum HMH stress (see Fig. 22). The selection of the resulting designs can be seen in the graph, method was inspired by pareto front [Ngatchou 2005].
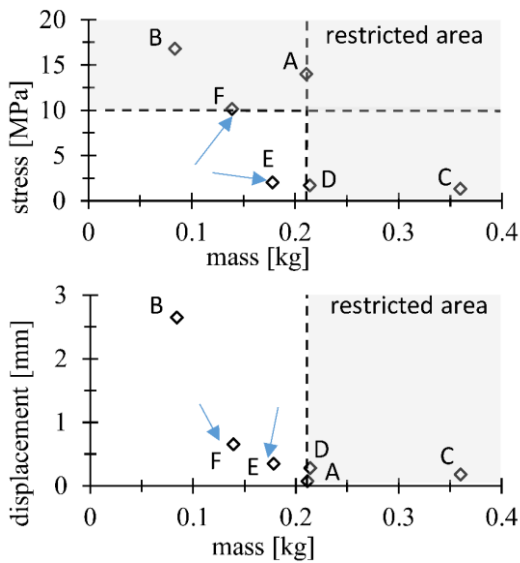

Figure 22. Two selected solution (marked by arrows).

Fig. 23, 24 illustrates two of the design shapes (E, F) as an example. The shape 'F' was already slightly beyond the allowed HMH equivalent stress, but for the needs of experiments we decided to produce it.
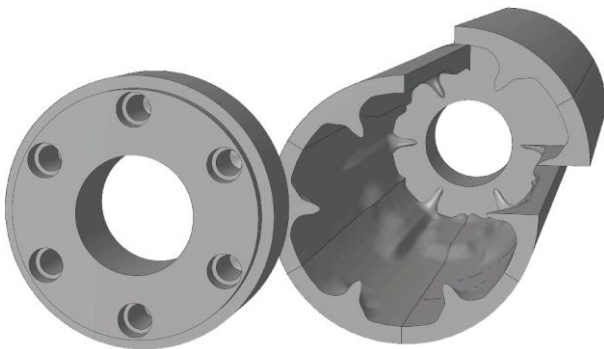

Figure 23. Optimized arm shape with weight 0.178 kg (shown in an exploded view to see the inner shape).
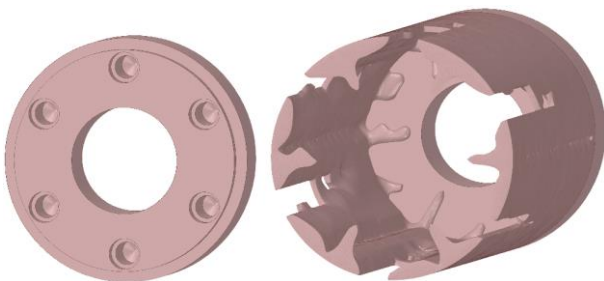

Figure 24. Optimized arm shape with weight 0.139 kg (shown in an exploded view to see the inner shape).

The two arm designs were printed using additive technology. These will be further used for mechanical tests in order to verify their functionality and comparison with the prediction from the FEM calculation. More will be mentioned in the next article. Fig. 25 shows a photograph of the manipulator arm that was printed on a Fortus 450mc machine [Fortus 2020].

Figure 25. Printed arm model with weight 0.139 kg.

8 DISCUSSION

The previous chapters showed the necessary steps to automate the optimization of the manipulator arm:

1) Determination of loading forces and their directions - this point is an input for topological optimization and at the same time it is often neglected or solved by a higher value of the safety factor.

2) Material model and its description - this point is also an input for topological optimization. It can be expected that it will be available, or it will be solved separately. This article is not primarily focused on determining the material model and its parameters, but a new article with this focus will be prepared.

3) Preparatory work - flanges, envelope design for topological optimization, etc. This step must be specified in advance. For example: The flanges are given by connecting elements and cannot be easily changed. The envelope for topological optimization is given by other design elements, e.g. necessary space for cables.

4) Topological optimization setting options are very wide, including symmetry, production technology etc. Several suggestions with different settings are presented in chapter 7.

5) The commercially available Ansys software [Ansys 2019] was used to finalize the model before printing (the procedure can be automated using e.g. a script).

6) The final shape of the arm was created on a 3D printing machine Fortus 450mc.

Determining the loading forces seems to be a critical point in the automation of arm design. This is not the aim of the solution, but in the case of poorly selected loads we get a bad result in topological optimization. The resulting behaviour may not meet the requirements. Other points seem to be algorithm able, although smoothing out the result of topological optimization is not ideal (see Fig. 23).

The above steps of the solution will be further developed within the project. These include identification of the material model and its parameters, creation of a script for automatic adjustment of the resulting geometry into printable form and preparation of a framework for solving the topological optimization itself.

9 CONCLUSION

The paper dealt with the problem of replacing the original aluminium (Al6061) arm of the ERC manipulator with a plastic (ABS-M30) arm produced with additive technology. This step makes sense in terms of arm manufacturing, especially in case of a piece production. Due to the increasing use of additive technology, this method of production may be more affordable.

First, it was necessary to determine the load acting on the manipulator arm, both in its static position and during its movement. Static load values were available and based on design guidelines for the competition for which the manipulator was designed. Dynamic load values were determined by measuring with 3-axis accelerometer at each manipulator movement.

Another point was the determination of material parameters (Young's modulus and Poisson number) of material ABS-M30. For this purpose, a total of 18 specimens (6 sets of 3 pieces) were printed with different orientations in printer chamber - different way of laying layers of material. These specimens were subjected to a tensile test in various configurations (6x simple tensile test; 6x graduated tensile test with a step size of 0.25 mm and a 1 min delay). The tests were also measured by the DIC method to determine the Poisson number. Tests have shown that in an area up to 10 MPa, the anisotropy of specimens (different printing orientations and material laying) will not significantly affect the material behaviour. For this reason, a value of 10 MPa was determined by the limiting condition for topological optimization. The Poisson number was $\mu = 0.33$ and the Young's modulus was determined to be $E = 1950$ MPa.

This was followed by topological optimization of the manipulator arm. The optimization was performed in the FEM program Ansys. The target function was the option of maximizing the stiffness of the model when the percentage weight was taken away. This approach appeared to be the best in terms of constraints.

ACKNOWLEDGMENTS

REFERENCES

[ERC 2020] European Rover Challenge [online]. 2020 [cit. 2020-02-26]. Available from: http://roverchallenge.eu/

[Dizon 2018] Dizon, J. R. C., et al. Mechanical characterization of 3D-printed polymers. Additive Manufacturing, 2018, 20: 44-67.

[Tafazoli 1999] Tafazoli, S., Lawrence, P. D. and Salcudean, S. E. Identification of inertial and friction parameters for excavator arms. IEEE transactions on robotics and automation, 1999, 15.5: 966-971.

[Corradini 2012] Corradini, M. L., Fossi, V., Giantomassi, A., et al. Discrete time sliding mode control of robotic manipulators: Development and experimental validation. Control Engineering Practice, 2012, 20.8: 816-822.

[Zhang 2007] Zhang, X., Mills, J. K. and Cleghorn, W. L. Dynamic modelling and experimental validation of a 3-PRR parallel manipulator with flexible intermediate links. Journal of Intelligent and Robotic Systems, 2007, 50.4: 323-340.

[Zhang 2018] Zhang, H., Cai, L., Golub, M., et al. Tensile, creep, and fatigue behaviours of 3D-printed acrylonitrile butadiene styrene. Journal of Materials Engineering and Performance, 2018, 27.1: 57-62.

[Duty 2018] Duty, C., Ajinjeru, C., Kishore, V., et al. What makes a material printable? A viscoelastic model for extrusion-based 3D printing of polymers. Journal of Manufacturing Processes, 2018, 35: 526-537.

[Schreier 2009] Schreier, H., Sutton, M. A. and Orteu, J. J. Image correlation for shape, motion and deformation measurements: Basic concepts, theory and applications. Boston, MA: Springer-Verlag US, 2009

[Sigmund 2013] Sigmund, O. and Maute, K. Topology optimization approaches. Structural and Multidisciplinary Optimization. 2013, 48(6), 1031-1055. DOI: 10.1007/s00158-013-0978-6. ISSN 1615-147X. Available from: http://link.springer.com/10.1007/s00158-013-0978-6

[Bensoe 2003] Bendsoe, M. P. and Sigmund, O. Topology optimization: theory, methods, and applications. New York: Springer, 2003. ISBN ISBN9783540429920

[Andreassen 2011] Andreassen, E., Clausen A., Schevenels M., et al. Efficient topology optimization in MATLAB using 88 lines of code, Structural and Multidisciplinary Optimization 43 (2011), no. 1, 1-16

[Ansys 2019] ANSYS, Inc. Products 2019 R3 documentation. https://www.ansys.com/, 2019. SAS IP, U.S.A

[Mohammed 2010] Mohammed, A. Q., Abuhadrous, I. and Elaydi, H. Modeling and Simulation of 5 DOF educational robot arm, 2010 2nd International Conference on Advanced Computer Control, Shenyang, 2010, pp. 569-574. doi: 10.1109/ICACC.2010.5487136

[Sobriety 2012] Optical measuring systems [in Czech]. Sobriety s.r.o. [online]. c2012-2020 [cit. 2020-02-21]. Available from: https://www.sobriety.cz/cs/opticke-merici-systemy

[Trebuna 2017] Trebuna, F., Hunady, R., Pastor, M., et al. Optical methods in mechanics [in Slovak]. Kosice: Edition of scientific and technical literature, 2017. ISBN 978-80-553-3168-3.

[Ngatchou 2005] Ngatchou, P.; Zarei, A., El-sharkawi, A. Pareto multi objective optimization. In: Proceedings of the 13th International Conference on, Intelligent Systems Application to Power Systems. IEEE, 2005. p. 84-91.

[Fortus 2020] Fortus 380mc and Fortus 450mc. Stratasys [online]. 2020 [cit. 2020-02-28]. Available from: https://www.stratasys.com/3d-printers/fortus-380mc-450mc.

CONTACTS:

Ing. Zbynek Paska
Department of Applied Mechanics
VSB – Technical University of Ostrava
Faculty of Mechanical Engineering
17. listopadu 2172/15
708 33 Ostrava – Poruba, Czech Republic
e-mail zbynek.paska@vsb.cz